2015

Phase transformation and magnetic properties of rapidly solidified Mn-Al-C alloys modified with Zr

Yunlong Geng
University of Nebraska–Lincoln, gengyunlong@gmail.com

Micheal J. Lucis
University of Nebraska–Lincoln

Pamela Rasmussen
Raymond Central High School

Jeffrey E. Shields
Raymond Central High School, University of Nebraska–Lincoln

Phase transformation and magnetic properties of rapidly solidified Mn-Al-C alloys modified with Zr

Yunlong Geng,[1,2,a)] Michael J. Lucis,[1,2] Pamela Rasmussen,[3] and Jeffrey E. Shield[1,2]
[1]*Department of Mechanical & Materials Engineering, University of Nebraska–Lincoln, Lincoln, Nebraska, USA*
[2]*Nebraska Center for Materials and Nanoscience, University of Nebraska–Lincoln, Lincoln, Nebraska, USA*
[3]*Raymond Central High School, Raymond, Nebraska, USA*

(Received 25 March 2015; accepted 12 July 2015; published online 20 July 2015)

$Mn_{54-x}Al_{43}C_3Zr_x$ (x = 1, 3) alloys were prepared by rapid solidification followed by heat treatment to produce the ferromagnetic τ phase. The substitution of Zr for Mn in the structure resulted in an increase of the saturation magnetization (M_s) compared to that of $Mn_{54}Al_{43}C_3$. While the highest M_s (128 ± 1 emu/g) was obtained in $Mn_{53}Al_{43}C_3Zr_1$, the coercivity was also improved to 1.62 kOe, compared to 1.25 kOe for $Mn_{54}Al_{43}C_3$. To further improve the coercivity through grain refinement, additional C (1%, 3%, 5%, and 7%) was added to $Mn_{53}Al_{43}C_3Zr_1$. An increase in the coercivity was observed due to a decrease of grain size and the formation of nonmagnetic phases, which reduced the magnetostatic interactions between the τ-phase grains. However, excess C reduced the saturation magnetization due to the formation of the other non-ferromagnetic phases, including ε, γ_2, and β phases. © *2015 AIP Publishing LLC*. [http://dx.doi.org/10.1063/1.4927289]

INTRODUCTION

Mn-Al-based permanent magnets, free from rare-earth elements, exhibit an excellent combination of magnetic and mechanical properties.[1,2] Due to the presence of the intermetallic tetragonal $L1_0$ phase (τ phase), it shows strong, uniaxial magnetocrystalline anisotropy energy with an "easy" c-axis. The τ phase is typically formed by quenching from the high-temperature hcp ε phase, followed by heat treatment at 450–600 °C.[3–5] Since the τ phase is metastable, prolonged annealing at elevated temperatures can lead to the transformation of τ phase to the stable but nonmagnetic γ (Al_8Mn_5) and β (Mn) phases.[6] The addition of a small amount of carbon into the MnAl alloy can stabilize the τ phase by inhibiting the decomposition of the τ phase.[7,8] The highest coercivity in C-added Mn-Al was obtained for carbon content just above the solubility limit of carbon.[9–11] Thus, the composition of $Mn_{54}Al_{43}C_3$ was used as reference composition in this research.

One shortfall of the τ-MnAl is its lower saturation magnetization, especially compared to Fe- or Co-based permanent magnets. While the Al layer in the $L1_0$ structure effectively increases the Mn-Mn distances (Fig. 1), resulting in ferromagnetic coupling, its presence dilutes the magnetization. Furthermore, the $L1_0$ phase in this system is hyperstoichiometric relative to Mn, as the minimum Mn content is governed by the composition of the ε phase from which τ forms. In τ phase $Mn_{54}Al_{46}$, 4% of the Mn atoms occupy Al sites, which couple antiferromagnetically with the Mn atoms in the Mn layers, resulting in a decrease in the saturation magnetization over stoichiometrically perfect $L1_0$.[2] Therefore, one approach to substitutional alloying is to replace the Mn atoms in the Al layer with non-magnetic atoms, which would effectively increase the magnetization. Alloying effects of several elements including Ti, Ni, Zn, Cu, B, Dy, and Pr in Mn-Al alloy have been studied.[12–15] A decrease in magnetization and constant coercivity was observed with a Ni addition;[12] an enhancement of coercivity from 1 kOe to 3 kOe and reduction in magnetization was caused by the addition of B;[12] the phase transformation to τ was depressed by the addition of Ti;[12] and Cu showed no influence on the magnetic properties of Mn-Al alloys.[12] A Mn-Al-Zn alloy, prepared by water quenching the induction-melted alloy followed by heat treatment at 420 °C for 1 h, showed an initial increase in magnetization at low Zn content and then a decrease at Zn content of more than 1.6 at. %. However, the overall magnetization of these Mn-Al-Zn alloys was as low as ~15 emu/g, compared to ~100 emu/g produced with other processing.[2] Substitution of rare-earth elements Pr and Dy slightly improved the magnetic properties, and the anisotropy constant enhancement was attributed to either the 3d–4f electron interactions or simply the

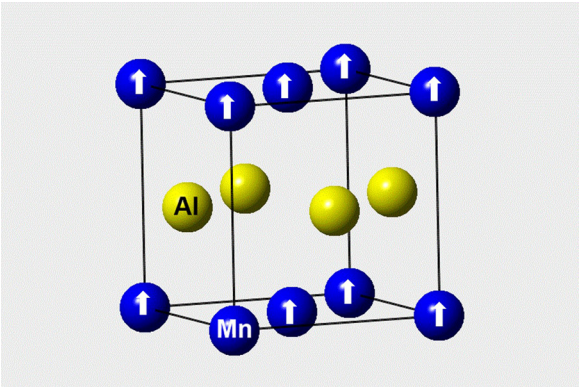

FIG. 1. Schematic illustration of perfect $L1_0$ structure for MnAl in τ phase.

a)Author to whom correspondence should be addressed. Electronic mail: gengyunlong@gmail.com. Tel.: +1(402)-770-6842; Fax: +1(402) 472-8292.

increase in atomic distance between Mn atoms. The alloying effect of Zr, with a similar electronegativity but larger atomic radius compared to Mn, has never been studied. Therefore, the introduction of Zr element into $Mn_{54}Al_{43}C_3$ was investigated in this research.

EXPERIMENTAL PROCEDURES

All ingots were prepared by arc melting high-purity (>99.97%) Mn, Al, C, and Zr elements in an Ar atmosphere. Melt spun ribbons (~50 μm in thickness, ~2 mm in width, and ranging from several centimeters to tens of centimeters in length) with compositions $Mn_{54-x}Al_{43}C_3Zr_x$ (x = 1, 3) and $(Mn_{53}Al_{43}C_3Zr_1)_{100-z}C_z$ (with z = 1, 3, 5, 7) were obtained by rapid solidification through a single-roller melt spinner at a tangential wheel speed of 40 m/s in an Ar atmosphere. The brittle as-solidified ribbons were hand-grounded in a mortar and pestle into powders for heat treatment and analysis. Heat treatment was conducted at 500 °C by sealing in quartz capsules after repeated evacuation/backfill cycles using ultrahigh purity Ar followed by water quenching to retain the τ phase. In order to follow the kinetics of the τ-phase formation and decomposition, each sample was annealed for a series of time increasing from 10 min to 60 min.

Crystal structure and microstructure characterization was performed by X-ray diffraction (XRD) (Rigaku Multiflex with Cu-Kα radiation). To minimize the background, an off-cut single-crystal Si slide was used as a sample holder. To determine the magnetic properties, the powders were embedded in epoxy resin and measured at room temperature using a Quantum Design Magnetic Property Measurement System (MPMS) superconducting quantum interference device magnetometer (SQUID) under a field of 7 T. No demagnetization correction was made for the magnetic measurements. The law of approach to saturation was utilized to estimate the saturation magnetization (M_s).[16] Briefly, this is accomplished by plotting M (magnetization) as a function of 1/H (H represents applied field) for H > 20 kOe and extrapolating the linear regression fit to 1/H = 0.

RESULTS AND DISCUSSION

The as-solidified phase formation for x = 0 revealed single-phase ε (Fig. 2). The addition of Zr slightly altered the solidification behavior, resulting in the formation of some minor phases and indicated by the low-intensity peaks at ~56°, 66°, and 82° 2θ (Fig. 3). These peaks are evident for both x = 1 and 3, and the intensity of this peak is slightly higher at x = 3. Since intensities of the peaks were too low and the peaks may be from multi phases, it was difficult to unequivocally identify the phases.

Heat treatment at 500 °C for 10 min was applied to all the as-solidified samples, which, for $Mn_{54}Al_{43}C_3$, typically results in the formation of the τ phase.[17] XRD patterns for the annealed $Mn_{54-x}Al_{43}C_3Zr_x$ (x = 0, 1, 3) revealed that the τ phase was the predominant phase, while a small fraction of ε and γ_2 phases were also observed, increasing in phase fraction as x increased (Fig. 3). The lattice parameters were

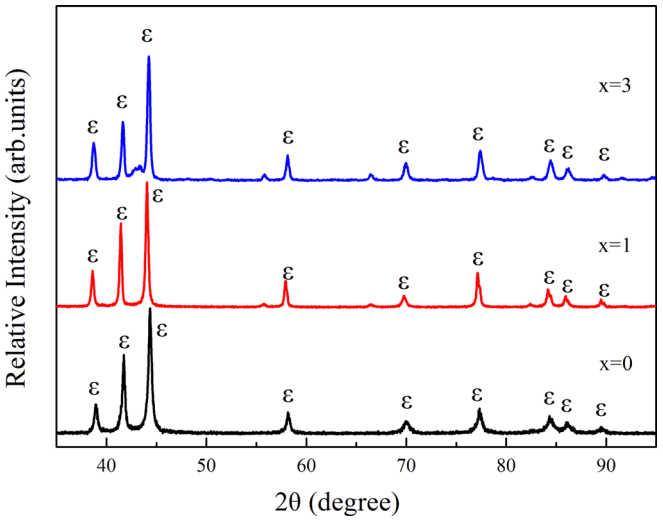

FIG. 2. XRD patterns for as-solidified $Mn_{54-x}Al_{43}C_3Zr_x$ (x = 0, 1, 3).

calculated with the first 5 Lorentz-shaped peaks after removal of the Kα_2 component. For x = 1, a = 3.912 ± 0.003 Å and c = 3.598 ± 0.005 Å were obtained. Compared to the lattice parameters for τ phase $Mn_{54}Al_{43}C_3$ (a = 3.901 ± 0.003 Å, c = 3.634 ± 0.004 Å), the c/a ratio decreased from 0.932 ± 0.002 to 0.923 ± 0.002. When the Zr content was increased to 3 at. %, the transformation of ε to τ phase was suppressed. Instead, ε, γ_2, and β phases were observed after heat treatment. Since the transformation from ε to τ phase is a massive transformation,[4] formation of τ phase nuclei with the same composition as the matrix is critical for the τ phase to compete with the formation of the equilibrium phases.[18]

The hysteresis loop for the $L1_0$-structured $Mn_{53}Al_{43}C_3Zr_1$ and $Mn_{54}Al_{43}C_3$ alloy is shown in Figure 4. The M_s and H_c for $L1_0$-structured $Mn_{54}Al_{43}C_3$ were reported to be 115 emu/g and 1.2 kOe, respectively.[17] In our experiment, the M_s and H_c for $Mn_{54}Al_{43}C_3$ were 115 emu/g and 1.4 kOe. In $Mn_{53}Al_{43}C_3Zr_1$, the M_s reaches as high as 128.0 ± 1 emu/g, even with a small fraction of impurity phases (ε phase and γ_2

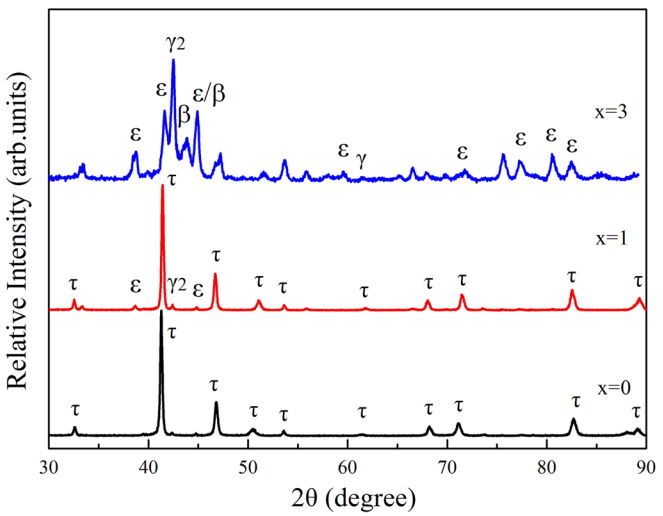

FIG. 3. XRD patterns for $Mn_{54-x}Al_{43}C_3Zr_x$ (x = 0, 1, 3) heat treated at 500° for 10 min.

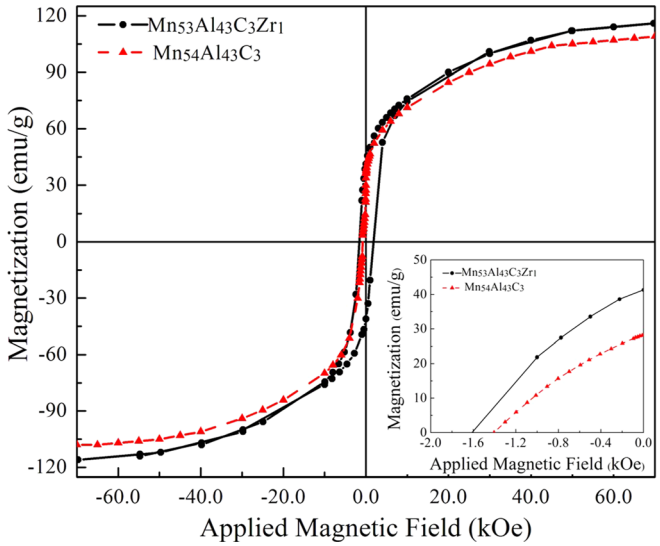

FIG. 4. Hysteresis loops for as-annealed $Mn_{53}Al_{43}C_3Zr_1$. The inset shows the coercivity and remanence in the 2nd quadrant.

phase). The increase in M_s could be due to the substitution of Zr to Mn in Al sites, suppressing the antiferromagnetic coupling and thus increasing the net magnetization. Also, some contribution to the increase in magnetization could conceivably be from inducing a magnetic moment on Zr, which has 2 unpaired electrons in the 4d shell. The H_c increased to 1.62 kOe with the addition of 1 at. % Zr, which could be due to changes in the magnetocrystalline anisotropy caused by the decrease of the c/a ratio. Since the coercivity is closely related to the microstructures, the increase in H_c with the addition of 1 at. % Zr could also be caused by microstructural changes, notably a decrease in grain size, during the formation of the τ phase. The grain size for $Mn_{53}Al_{43}C_3Zr_1$ was determined by the Scherrer equation $d = \frac{k\lambda}{B_0 \sin\theta}$, where d is the mean grain size, k is a constant (usually taken as 1), θ the Lorentz-shaped Bragg angle, λ the wavelength of incident x-radiation in nm, and B_0 the instrument-corrected FWHM of the diffraction peak of interest (in this case, (101)).[19] The grain size was ~45 nm, while it was ~500 nm (Ref. 11) for $Mn_{54}Al_{43}C_3$.

In order to maximize the energy product of $Mn_{53}Al_{43}C_3Zr_1$, the enhancement of the saturation magnetization should be coupled with an increase in coercivity, as the coercivity should be at least $M_s/4$ for applications. Here, the M_s is 8 kG, so the observed coercivity is slightly smaller than $M_s/4$. Thus, further improvement in coercivity would ensure usefulness, particularly at temperatures above room temperature. Here, further improvements in coercivity were attempted through microstructural modification. In magnetic materials, the microstructure, particularly the grain size, plays a critical role in maximizing the extrinsic coercivity.[11,20] Grain refinement can be facilitated by two factors: number and potency of the nucleation sites, and solute elements present in the melt that retards grain growth.[21–23] Carbon additions could increase the number of nucleation sites or may tend to segregate, restricting grain growth during the solidification process. Therefore, additional amounts of C (1%, 3%, 5%, and 7%) were added to the $Mn_{53}Al_{43}C_3Zr_1$ alloys to study the effects on microstructural development.

XRD patterns for as-solidified $(Mn_{53}Al_{43}C_3Zr_1)_{100-z}C_z$ (with $z = 0, 1, 3, 5, 7$) were indexed to the ε phase. In contrast to the Zr-free alloys and the alloys without excess C where conversion from ε to τ occurred readily after heat treatment at 500 °C for 10 min, excess C appeared to alter the decomposition kinetics. In as-solidified $(Mn_{53}Al_{43}C_3Zr_1)_{95}C_5$, the ε phase was retained until heat treatment for 30 min when a large fraction of τ phase and a small amount of ε phase was observed (Fig. 5). Heat treatment at 500 °C for 40 min did not noticeably increase the τ phase fraction, but after heat treatment at 500 °C for 60 min, in addition to τ and ε, the equilibrium γ_2 and β phases were also observed, indicating that complete conversion from ε to τ is not possible before decomposition to the equilibrium phases occurs. To obtain a larger fraction of the τ phase, variable annealing time (10 min, 30 min, 40 min, and 60 min) was applied to each as-solidified sample. The annealing time to produce the largest fraction of τ phase is defined here as "optimum time," which is represented by the largest $I' = I_\tau/(I_\varepsilon + I_{\gamma 2} + I_\beta)$, where I_τ is the intensity for (101) peak in τ phase, I_ε is the intensity for (100) peak in ε phase, $I_{\gamma 2}$ is the intensity for (330) peak in γ_2 phase, and I_β is the intensity for (411) peak in β phase. For example, for $(Mn_{53}Al_{43}C_3Zr_1)_{95}C_5$, the values of I' calculated from the data shown in Fig. 5 are 0, 13 ± 2, 31 ± 5, and 2.0 ± 0.1 for samples annealed for 10 min, 30 min, 40 min, and 60 min, respectively. Thus, the "optimum time" is 40 min. Based on this calculation, the "optimum time" changes with C content are shown in Fig. 6. When the amount of C (z) was increased from 1 to 7, the heat treatment time to maximize τ formation (i.e., "optimum time") increased from 10 min to 60 min. XRD patterns for annealed $(Mn_{53}Al_{43}C_3Zr_1)_{100-z}C_z$ ($z = 0$, 1, 3, 5, 7) are shown in Fig. 7. The τ phase was determined to be the primary phase in annealed $(Mn_{53}Al_{43}C_3Zr_1)_{100-z}C_z$ ($z = 0$, 1, 3, 5, 7) samples, while ε, γ_2, and β phases were found as minor phases.

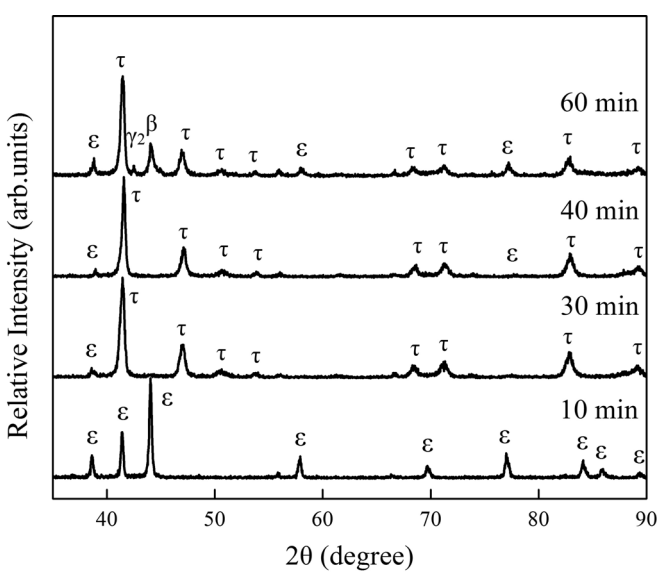

FIG. 5. XRD patterns for $(Mn_{53}Al_{43}C_3Zr_1)_{95}C_5$ with variable annealing time ($t = 10, 30, 40, 60$ min).

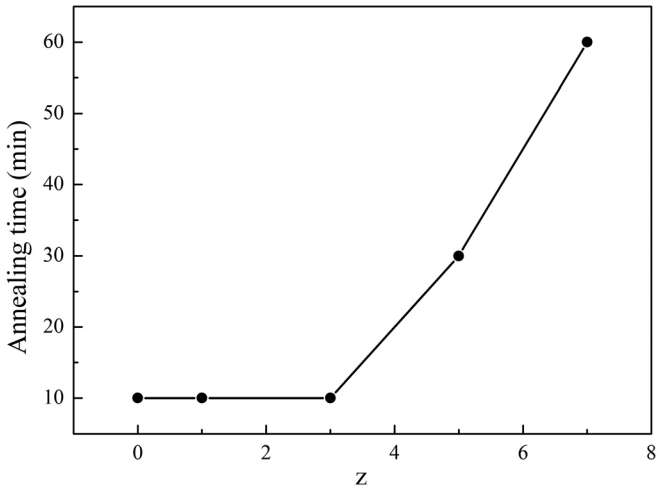

FIG. 6. Optimum annealing time for samples $(Mn_{53}Al_{43}C_3Zr_1)_{100-z}C_z$ (with z = 0, 1, 3, 5, 7).

Annealing the $(Mn_{53}Al_{43}C_3Zr_1)_{93}C_7$ at 500 °C for 60 min produced primarily τ phase with small amounts of ε, γ_2, and β phases, indicating that the τ phase in $(Mn_{53}Al_{43}C_3Zr_1)_{93}C_7$ was much more stable than in the case of $(Mn_{53}Al_{43}C_3Zr_1)_{95}C_5$. This could be explained by the transformation from τ phase to ε, γ_2, and β phases, which is a diffusion-controlled process and involves nucleation and growth. The increase in stability with C content occurs because the excess C atoms, likely segregated to grain boundaries, inhibit the diffusion of the Mn and Al atoms necessary for decomposition. Thus, C suppressed the phase transformation process from ε phase to τ phase and stabilizes the τ phase.

The grain sizes for $(Mn_{53}Al_{43}C_3Zr_1)_{100-x}C_x$ (x = 0, 1, 3, 5, 7) were determined by the Scherrer equation. As shown in Fig. 8, the overall trend of the grain size with the amount of C was clear. A decrease of grain size from around 45 nm to 25 nm with C addition up to 7% (z = 7) was observed, although the grain size when z = 7 is larger than that when z = 5.

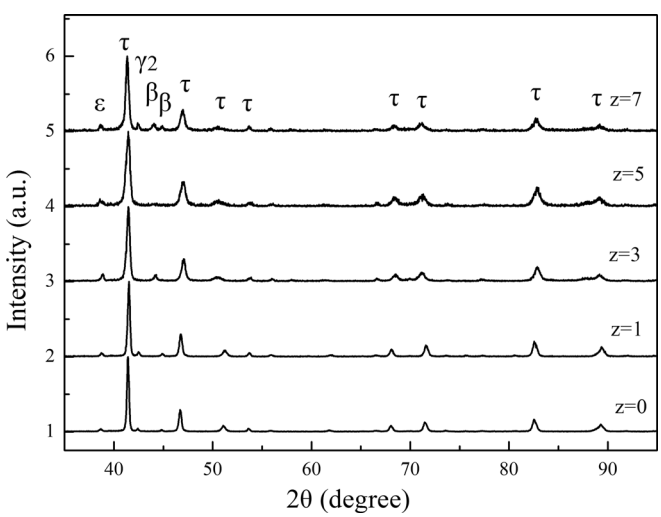

FIG. 7. XRD patterns for annealed $(Mn_{53}Al_{43}C_3Zr_1)_{100-x}C_x$ (x = 0, 1, 3, 5, 7).

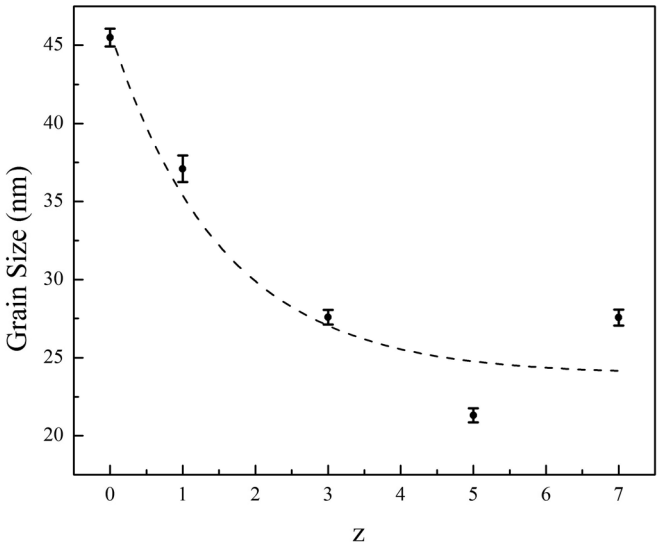

FIG. 8. Dependence of grain size in $(Mn_{53}Al_{43}C_3Zr_1)_{100-z}C_z$ (z = 0, 1, 3, 5, 7) on C content.

Influence of C addition in $(Mn_{53}Al_{43}C_3Zr_1)_{100-z}C_z$ (z = 0, 1, 3, 5, 7) on the magnetic properties, including coercivity (H_c) and saturation magnetization (M_s), is shown in Figs. 9 and 10. The effect of C content on M_s is clearly evident. A decrease of saturation magnetization from 128 emu/g to about 100 emu/g was observed, most likely due to the formation of nonmagnetic ε, γ_2, and β phases as determined by the XRD. Since the τ phase is the only ferromagnetic phase in the MnAl system, the M_s is proportional to the percentage of τ phase in the alloys. The coercivity shows an opposite trend with C addition as the saturation magnetization. This may be explained by the lower dependence of H_c on the amounts of τ phase and more on the microstructure. The coercivity increased even for z = 7, with a slightly larger grain size than z = 5. This could be due to the increasing amount of ε, γ_2, and β phases at the grain boundaries of τ phase, which would decouple the τ-MnAl grains. The maximum H_c (3.1 kOe) was obtained in $(Mn_{53}Al_{43}C_3Zr_1)_{93}C_7$.

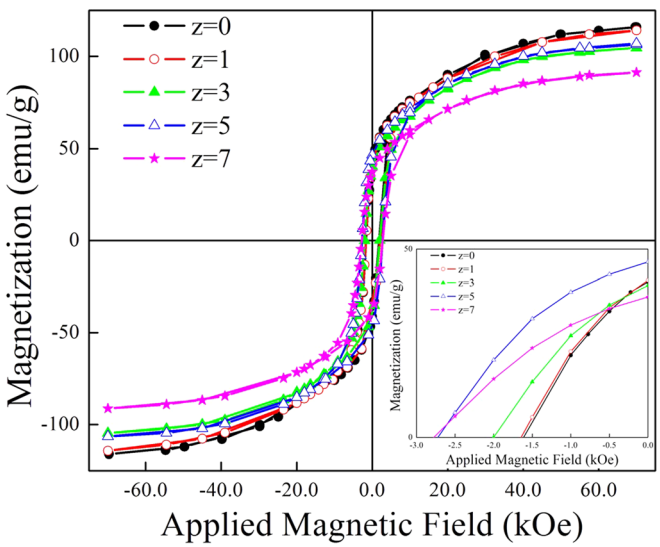

FIG. 9. Hysteresis loops for as-annealed $(Mn_{53}Al_{43}C_3Zr_1)_{100-z}C_z$ (z = 0, 1, 3, 5, 7). The inset shows the coercivity and remanence in the 2nd quadrant.

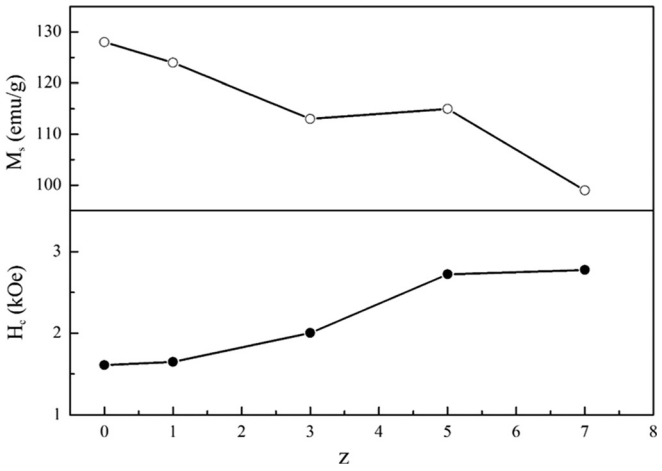

FIG. 10. Dependence of coercivity (H_c) and saturation magnetization (M_s) on carbon content in $(Mn_{53}Al_{43}C_3Zr_1)_{100-z}C_z$ ($z = 0, 1, 3, 5, 7$).

CONCLUSION

As-solidified $Mn_{53}Al_{44}C_3$ alloys with 1 at. % Zr addition exhibited a single-phase structure consisting of the ε phase. After heat treatment at 500 °C for 10 min, transformation from ε to τ phase was achieved with a higher saturation magnetization (128.0 ± 1 emu/g) and coercivity (1.62 kOe). To maximize its energy product, further enhancement of coercivity in $Mn_{53}Al_{43}C_3Zr_1$ was accomplished through grain refinement. The addition of C ($\sim$5 at. %) reduced the grain size from 45 nm to 25 nm, resulting in an increase of coercivity. However, the extra C resulted in the formation of room-temperature equilibrium phases, including ε, γ_2, and β phases. These phases decoupled the τ-phase grains, which improved the coercivity with increasing C from 5 at. % to 7 at. %. A decrease of saturation magnetization with the increasing amount of C resulted from the formation of these equilibrium phases, as only the τ phase is ferromagnetic and the other phases cause a dilution of magnetization.

ACKNOWLEDGMENTS

The authors gratefully acknowledge research support from the Department of Energy through the ARPA-E REACT program under Grant No. 0472-1537. The authors are also grateful for facility support from the Nebraska Research Initiative through the Nebraska Center for Materials and Nanoscience at the University of Nebraska.

[1]A. Koch, P. Hokkeling, and K. de Vos, "New material for permanent magnets on a base of Mn and Al," J. Appl. Phys. **31**, S75–S77 (1960).
[2]J. Park, Y. Hong, S. Bae, J. Lee, J. Jalli, G. Abo, N. Neveu, S. Kim, C. Choi, and J. Lee, "Saturation magnetization and crystalline anisotropy calculations for MnAl permanent magnet," J. Appl. Phys. **107**, 09A731 (2010).
[3]J. Van Den Broek, H. Donkersloot, G. Van Tendeloo, and J. Van Landuyt, "Phase transformations in pure and carbon-doped $Al_{45}Mn_{55}$ alloys," Acta Metall. **27**, 1497–1504 (1979).
[4]C. Yanar, J. Wiezorek, W. Soffa, and V. Radmilovic, "Massive transformation and the formation of the ferromagnetic L10 phase in manganese-aluminum-based alloys," Metall. Mater. Trans. A **33**, 2413–2423 (2002).
[5]Y. Kurtulus and R. Dronskowski, "Electronic structure, chemical bonding, and spin polarization in ferromagnetic MnAl," J. Solid State Chem. **176**, 390–399 (2003).
[6]T. B. Massalski, H. Okamoto, P. Subramanian, and L. Kacprzak, *Binary Alloy Phase Diagrams* (ASM International, 1990).
[7]L. Pareti, F. Bolzoni, F. Leccabue, and A. Ermakov, "Magnetic anisotropy of MnAl and MnAlC permanent magnet materials," J. Appl. Phys. **59**, 3824–3828 (1986).
[8]E. Fazakas, L. Varga, and F. Mazaleyrat, "Preparation of nanocrystalline Mn–Al–C magnets by melt spinning and subsequent heat treatments," J. Alloys Compd. **434**, 611–613 (2007).
[9]Q. Zeng, I. Baker, J. Cui, and Z. Yan, "Structural and magnetic properties of nanostructured Mn–Al–C magnetic materials," J. Magn. Magn. Mater. **308**, 214–226 (2007).
[10]J. Le Breton, J. Bran, E. Folcke, M. Lucis, R. Lardé, M. Jean, and J. Shield, "Structural modifications in a $Mn_{54}Al_{43}C_3$ melt-spun alloy induced by mechanical milling and subsequent annealing investigated by atom probe tomography," J. Alloys Compd. **581**, 86–90 (2013).
[11]M. J. Lucis, T. E. Prost, X. Jiang, M. Wang, and J. E. Shield, "Phase transitions in mechanically milled Mn-Al-C permanent magnets," Metals **4**, 130–140 (2014).
[12]Y. Sakka, M. Nakamura, and K. Hoshimoto, "Rapid quenching and properties of hard magnetic materials in MnAl-X (X= Ti, Cu, Ni, C, B) systems," J. Mater. Sci. **24**, 4331–4338 (1989).
[13]H. Wang, P. Si, W. Jiang, J. Lee, C. Choi, J. Liu, Q. Wu, M. Zhong, and H. Ge, "Structural stabilizing effect of Zn substitution on MnAl and its magnetic properties," Open J. Microphys. **1**, 19 (2011).
[14]H. X. Wang, P. Z. Si, W. Jiang, X. F. Xiao, J. G. Lee, C. J. Choi, M. Zhong, Z. F. Li, and H. L. Ge, "Structure and magnetic properties of Cu doped MnAl," Phys. Sci. Int. J. **4**, 536–541 (2014).
[15]Z. Liu, C. Chen, Z. Zheng, B. Tan, and R. V. Ramanujan, "Phase transitions and hard magnetic properties for rapidly solidified MnAl alloys doped with C, B, and rare earth elements," J. Mater. Sci. **47**, 2333–2338 (2012).
[16]W. F. Brown, "Theory of the approach to magnetic saturation," Phys. Rev. **58**, 736–743 (1940).
[17]T. E. Prost, "Magnetic properties study of the Mn-Al system with additions of B or C and mechanical milling techniques," Ph.D. dissertation (University of Nebraska–Lincoln, 2012).
[18]H. Aaronson, "Mechanisms of the massive transformation," Metall. Mater. Trans. A **33**, 2285–2297 (2002).
[19]A. Patterson, "The Scherrer formula for X-ray particle size determination," Phys. Rev. **56**, 978 (1939).
[20]W. Rave and K. Ramstöck, "Micromagnetic calculation of the grain size dependence of remanence and coercivity in nanocrystalline permanent magnets," J. Magn. Magn. Mater. **171**, 69–82 (1997).
[21]A. K. Dahle, Y. C. Lee, M. D. Nave, P. L. Schaffer, and D. H. StJohn, "Development of the as-cast microstructure in magnesium–aluminium alloys," J. Light Metals **1**, 61–72 (2001).
[22]Y. Lee, A. Dahle, D. StJohn, and J. Hutt, "The effect of grain refinement and silicon content on grain formation in hypoeutectic Al–Si alloys," Mater. Sci. Eng., A **259**, 43–52 (1999).
[23]Q. Jin, J.-P. Eom, S.-G. Lim, W.-W. Park, and B.-S. You, "Grain refining mechanism of a carbon addition method in a Mg–Al magnesium alloy," Scr. Mater. **49**, 1129–1132 (2003).